SANDIA REPORT

SAND99–0739
Unlimited Release
Printed April 1999

Laser Spray Fabrication for Net-Shape Rapid Product Realization LDRD

C. L. Atwood, M. L.Griffith, L. D. Harwell, D. L. Greene, D. E. Reckaway, M. T. Ensz, D. M. Keicher, M. E. Schlienger, J. A. Romero, M. S. Oliver, F. P. Jeantette, J. E. Smugeresky

Prepared by
Sandia National Laboratories
Albuquerque, New Mexico 87185 and Livermore, California 94550

Sandia is a multiprogram laboratory operated by Sandia Corporation, a Lockheed Martin Company, for the United States Department of Energy under Contract DE-AC04-94AL85000.

Sandia National Laboratories

Issued by Sandia National Laboratories, operated for the United States Department of Energy by Sandia Corporation.

Available to DOE and DOE contractors from
Office of Scientific and Technical Information
P.O. Box 62
Oak Ridge, TN 37831

Prices available from (703) 605-6000
Web site: http://www.ntis.gov/ordering.htm

Available to the public from
National Technical Information Service
U.S. Department of Commerce
5285 Port Royal Rd
Springfield, VA 22161

NTIS price codes
Printed copy: A03
Microfiche copy: A01

SAND99-0739
Unlimited Release
Printed April 1999

LASER SPRAY FABRICATION FOR NET-SHAPE RAPID PRODUCT REALIZATION LDRD

C. L. Atwood, M. L. Griffith, L.D. Harwell,
D.L. Greene, D. E. Reckaway, M. T. Ensz,
Mechanical Engineering Dept.

D. M. Keicher, M. E. Schlienger, J. A. Romero,
M. S. Oliver, F. P. Jeantette
Direct Fabrication Dept.

Sandia National Laboratories
P.O. Box 5800
Albuquerque, NM 87185-1484

J. E. Smugeresky
Materials Reliability Dept.
Sandia National Laboratories
P.O. Box 969
Livermore, CA 94551-0969

Abstract

The primary purpose of this LDRD project was to characterize the laser deposition process and determine the feasibility of fabricating complex near-net shapes directly from a CAD solid model. Process characterization provided direction in developing a system to fabricate complex shapes directly from a CAD solid model. Our goal for this LDRD was to develop a system that is robust and provides a significant advancement to existing technologies (e.g., polymeric-based rapid prototyping, laser welding).

Development of the process will allow design engineers to produce functional models of their designs directly from CAD files. The turnaround time for complex geometrical shaped parts will be hours instead of days and days instead of months. With reduced turnaround time, more time can be spent on the product-design phase to ensure that the best component design is achieved. Maturation of this technology will revolutionize the way the world produces structural components.

This Page Is Intentionally Left Blank.

Contents

Figures

INTRODUCTION

Laser Spray Fabrication for Net-Shape Rapid Product Realization now known as Laser Engineered Net Shaping (LENS™) is a new manufacturing process for fabricating metal parts directly from a Computer Aided Design (CAD) solid model. The process is similar to rapid prototyping technologies in its approach to fabricate a solid component by layer additive methods. However, the LENS™ technology is unique in that fully dense metal components with material properties that are similar to that of wrought materials can be fabricated. The LENS™ process has the potential to dramatically reduce the time and cost required to realize functional metal parts. In addition, the process can fabricate complex internal features not possible using existing manufacturing processes.

The purpose of this LDRD project is to characterize the LENS™ process and determine the feasibility of fabricating complex, fully dense, metal parts directly from a CAD solid model. The goal of the LDRD is to verify that the material properties of the metal parts produced by the LENS™ process can be used to fabricate weapon components and begin the development of a robust, reliable, and predictable process. This will be accomplished using a systematic approach beginning with the fabrication and testing of simple geometries and progressing to more complex parts. Optimization of system hardware and software and the development of a parameter database will enable the success of the research and development effort.

PROCESS CHARACTERIZATION

INTRODUCTION

Lasers have gained wide spread acceptance over the last two decades as a useful tool for industrial materials processing applications. Laser cladding of similar and/or dissimilar materials for improved wear properties, corrosion resistance, thermal barrier coatings, etc., has been investigated extensively [1-4]. Models have been developed to describe some of the physical phenomenon that occur during the laser-cladding process [5,6]. Other studies have been performed to investigate process interactions, such as the laser absorption by the metal powder [7], and to measure the surface temperature of the cladding layer during processing [8]. More recently, the explosive growth in the area of rapid prototyping has prompted several groups to investigate the feasibility of using a process similar to the laser-cladding process for producing solid metal objects [9, 10]. As far back as 1984, the concept of using laser power or wire deposition to rebuild and/or produce solid geometries has existed [11].

Akin to "three-dimensional laser welding," we are developing a process called Laser Engineered Net Shaping (LENS™). This process allows complex three-dimensional solid metallic objects to be directly fabricated from a CAD solid model. Currently, this process functions similar to a stereolithography process. A faceted file is generated from the CAD solid model and then sliced into a sequence of layers. The sliced file is then input into another interpreter program that converts the sliced file into a series of tool path patterns required to build the entire layer. The component is fabricated by first generating an outline of the key component features and then filled using a rastering technique. This file is then used to drive the laser system to produce the desired component one layer at a time. This process differs from state-of-the-art rapid prototyping (RP) processes in that a fully dense, metallic component can be produced using this system.

Initially it was important to obtain a fundamental understanding of the LENS™ process. Experiments were performed to identify the process parameters that affect the LENS™ process variability. The results of these experiments have been used to develop response surface models for process optimization [12] and then to identify process control methodologies. The results of these experiments are reported below.

EXPERIMENTAL

Two laser systems have been used to develop the LENS™ process. The research platform consists of:

- an 1.8 kW CW Nd:YAG laser,
- a controlled atmosphere glove box,
- a 4-axis computer-controlled positioning system, and
- a powder feed unit.

The applications platform consists of:

- a 500W CW Nd:YAG laser,
- a controlled-atmosphere glove box,
- a 3-axis computer controlled positioning system, and
- a powder feed unit.

The positioning stages were mounted inside a controlled-atmosphere glove box operating at a nominal oxygen level of 2-3 parts per million. The glove-box atmosphere was Ar. The beam is brought into the glove box through a window mounted on the top of the glove box and directed to the deposition region using a six-inch focal length plano-convex lens. The powder delivery nozzle is designed to inject the powder stream directly into the focused laser beam. The lens and powder nozzle move as an integral unit.

A schematic representation of the LENS™ process is shown in Figure 1. The laser beam is focused onto a solid substrate, used as base for building an object, to create a molten puddle. The substrate is generally the same material as the powder being deposited. Powder particles are simultaneously injected into the puddle to build-up each layer. The substrate is moved beneath the laser beam to deposit thin metal lines to create the desired geometry for each layer. After deposition of each layer, the powder delivery nozzle and focus lens assembly is incremented away from the substrate a distance equal to the layer thickness to maintain a constant focus position. The powder is delivered to the deposition region via a carrier gas, and the powder volume is regulated by a powder-feed unit.

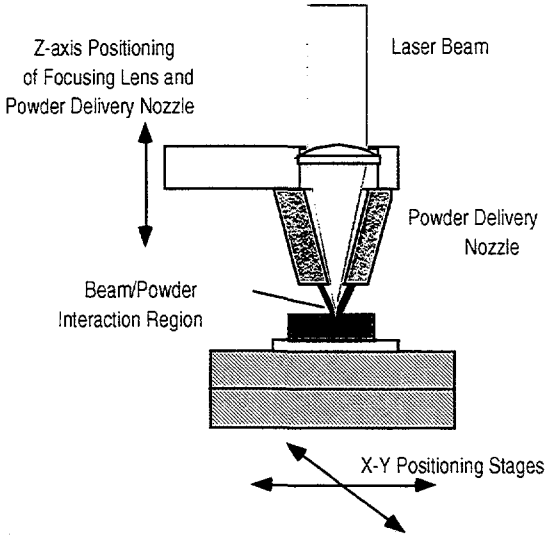

Figure 1. Configuration used in performing powder deposition experiments.

Experiments were performed on a variety of materials of which most were metals. Statistically designed experiments were done using Inconel™ 625 to identify significant

process variables and to begin to understand the deposition process. A list of the process variables considered for these experiments is given in Table 1.

Table 1. Process variables considered for statistically designed experiments.

Input Variable	Low	Medium	High
Laser Irradiance (W/mm^2)	345	549	774
Travel Speed (mm/s)	8.47	21.17	33.87
Z-Axis Incremen (mm)	0.127	0.229	0.381
Powder Volume (gm/min.)	1.785	2.418	3.057
Carrier Gas Pressure (MPa)	0.14	-	0.21
Powder Velocity (mm/s)	5000	-	6500

The response variables used in evaluating the experimental results were:

- the material build-up height,
- the melt depth into the previous layer, and
- the ratio of these two variables.

The tests were performed by depositing ten layers of metal in a single wall for each of the experimental conditions. The material was deposited in only one direction of travel. Diagnostics used during this experimentation included:

- laser Doppler velocimetry,
- time resolved infrared imaging,
- high magnification, high-speed digital imaging, and
- standard video imaging.

Metallography and electron microprobe analyses were performed to measure the response variables and to evaluate the experiment results. These results were then used to develop relationships for deposition interactions. Two powder mesh sizes were used for the alloy 625 experiments. All of the build-up experiments were performed using a -80 to +325 mesh, while a -325 mesh size powder was included in the high-speed imaging tests to observe the effect of powder particle size on the deposition process in the powder/beam interaction zone.

A Kodak Ektapro™ intensified and gated high-speed digital imaging system was used to slow down the deposition process and allow observation of the beam/powder interaction in the deposition region, perpendicular to the growth direction (in the X-Y plane). To view through the intense laser plume, a 150 mW, 690 nm wavelength diode laser was used as an illumination source. A laser line filter was placed in the lens to filter

out the broadband emission from the plume. For the high-speed photography, two different powder sizes were used to observe the effect of powder size on the performance of the process. The powder size distributions for the two powders were 50-180 μm for the larger powder size and <50 μm for the smaller powder size. The framing rate on the camera was 2000 pictures per second. A gate width of 50 μs was used at magnification of approximately 50x. The high-speed photography results were also used to identify whether significant heating of the powder particles occurred prior to impingement into the deposition melt zone.

RESULTS AND DISCUSSION

For the experiments using the Inconel™ 625 material, complete melting of the powder occurred for all the tests. In addition, textured grain growth of the deposited material occurred across the deposition layer boundary in nearly all cases. As mentioned previously, the two response variables considered for these tests were the material build-up height and the melt depth into the substrate. After the experiments were performed, metallographic cross sections of all of the test samples were made. The response variables were measured from photographs taken of these metallographic cross sections. The build-up height was measured from the original surface to the top of the deposited structure. Similarly, the melt depth was taken to be the depth of the dissolution region. A typical structure is shown in Fig. 2(a) for the deposition occurring at 345 W/mm^2, 8.47 mm/s travel speed, a powder volume of 1.9 gm/min, a gas pressure of 0.14 MPa and a z-axis increment of 0.381 mm/pass. Figure 2(b) shows the melt zone/substrate interface for the highest energy input parameters used in these experiments (774 W/mm^2, 1.9 gm/min. powder, 0.14 MPa carrier gas, 8.47 mm/s, z-increment 0.254 mm/pass). As can be seen from Fig. 2(b), there was very little intergranular melting in the substrate region. The intergranular melting that has occurred (indicated by arrow), goes into the substrate only a fraction of the substrate grain size. This suggests that for the conditions used in this testing, the heat-affected zone is relatively small.

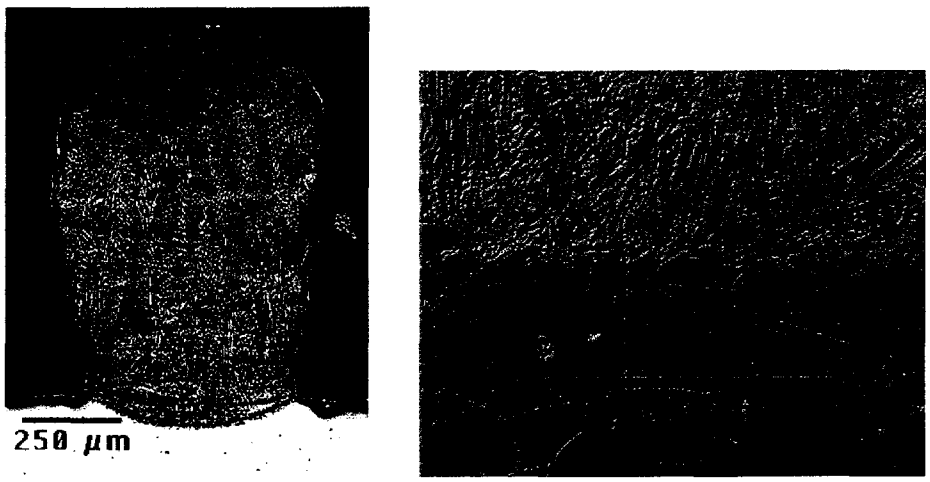

Figure 2. Photomicrographs showing: (a) textured grain growth for laser deposited materials and (b) melt-zone/substrate interface for the highest energy input parameters.

Figure 3 shows the melt depth into the substrate plotted as a function of the build-up height. For the experimental conditions used in these tests, the melt depth varied from a minimum depth of 0.048 mm to a maximum depth of 0.273 mm. The build-up height varied from a minimum of 0.071 mm to a maximum of 1.730 mm. The data sets are identified by the laser power and travel speed associated with each condition. As shown in Figure 3, the melt depth tends to increase with increasing laser power. As expected, the minimum melt depth occurs for the lowest laser power conditions, while the maximum melt depth tends to occur for the higher laser power conditions. There is, however, a great deal of overlap in the melt depth conditions for the intermediate and high-power parameters. At all of the power levels, there is a significant increase in build-up of the deposited material as the component travel speed is decreased, with only a modest increase in the melt depth at that power. In general, the trend from this cursory analysis suggests that the penetration into the substrate occurs early in the deposition process. If the part is scanned under the beam at a slow rate of speed, then the powder is given time to build and slightly more penetration occurs due to the slow travel speed. Conversely, if the substrate is scanned under the beam at a high rate of speed, the penetration into the substrate is affected little and the build-up is inhibited. In any case, it is apparent that minimum penetration into the substrate occurs when the irradiance is low, yet sufficient to incur complete melting.

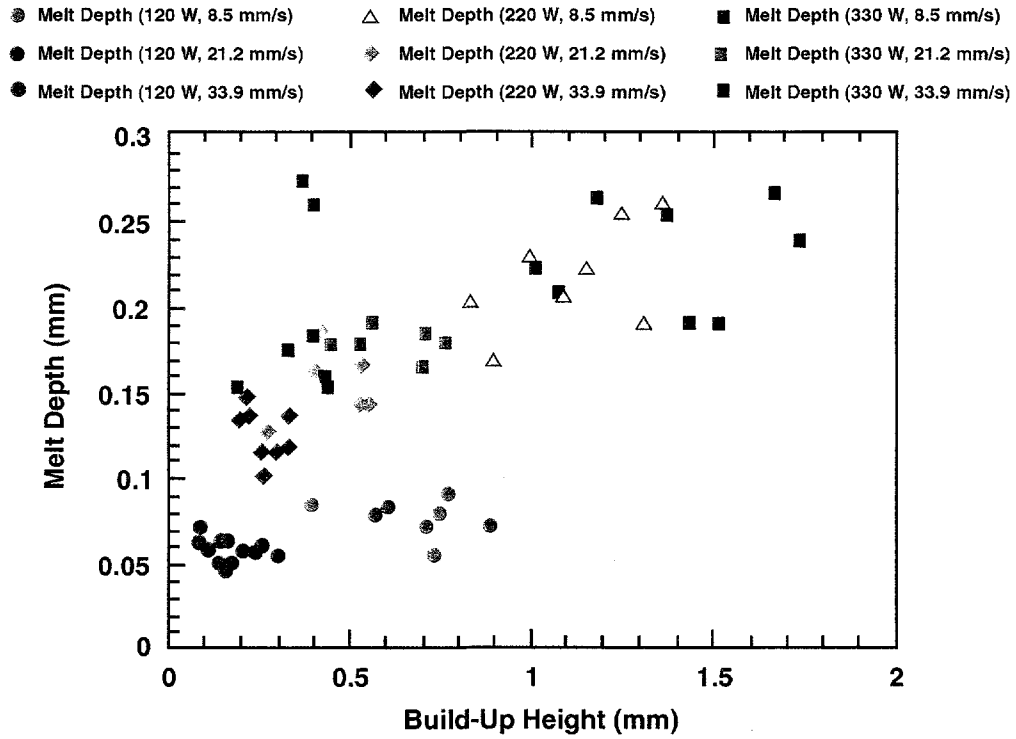

Figure 3. Measured results for melt depth and build-up height from experiment test matrix.

Although visual analysis of the sample cross sections exhibited no obvious signs of porosity, electron microprobe analysis was performed using wavelength dispersive

spectroscopy on selected samples at the test matrix extremum points to quantify this observation. Electron microprobe analysis provided a full-quantitative analysis of the material density in both the substrate and deposited material and compared these measurements to those from a known standard. The results suggested that the density of the deposited material was slightly denser than the substrate. They also indicated that there was no apparent difference in composition between the deposited material and the original substrate.

The data sets generated were analyzed using Minitab, a statistical data analysis package, to develop response surface models for the LENS™ process. The software allows the user to identify statistically significant factors for process optimization. In-depth results from this study are reported elsewhere [12]; however, what these experiments showed was that, for the factor space considered, laser irradiance and component velocity both played a significant role in the build-up and remelt processes. From these experimental results (see Figure 3), it is obvious that reducing the laser irradiance subsequently reduces the melt depth into the substrate. However, this also reduces the build-up rate. Further analysis of these experimental results suggests that there was strong correlation of the material build-up height to the total volumetric exposure (laser irradiance/component velocity). In fact, height increases were nearly linear with increasing exposure (see Figure 4).

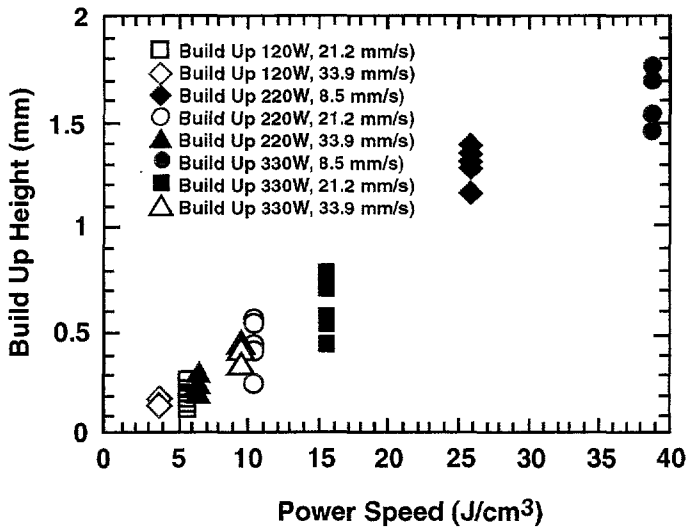

Figure 4. Plot of material build-up height vs. volumetric exposure for statistical designed experiment using Inconel™ 625 alloy.

High-speed, high-magnification imaging allowed the LENS™ process to be effectively slowed down to visualize the molten metal/powder interaction region. The laser illumination eliminated the broadband emission associated with the laser-generated plume and actually permitted the molten region to be observed for qualitative analysis. For both particle sizes, it appears that particles do not become molten until they are, in fact, actually injected into the melted metal puddle in the deposition region. For the smaller particle-size distribution, the melt puddle appeared to be stable and well behaved. For the larger particle size, however, the molten puddle was very energetic and unstable.

For the larger powder-size distribution, the particle size was a significant fraction of the deposition region width. Directing the larger particles into the molten deposition region caused a larger displacement of the liquid metal thus adding more energy to the oscillations of the melt pool. Further studies are required to draw more quantitative conclusions for the effects of particle size on the powder deposition process.

CONCLUSIONS FOR PROCESS CHARACTERIZATION

These experiments, as well as others [12], revealed that powder-feed rate, laser power, and traverse velocity are the main variables that control the LENS™ process. From these initial characterization experiments, we were able to continue development into solid component fabrication.

FABRICATION OF COMPONENTS AND THEIR PROPERTIES

INTRODUCTION

Solid free-form fabrication is one of the fastest growing automated manufacturing technologies that has significantly impacted the length of time between initial concept and actual part fabrication [13,14]. Starting with CAD renditions of new components, several techniques such as stereolithography [15] and selective laser sintering[16] are being used to fabricate highly accurate complex three-dimensional concept models using polymeric materials. Coupled with investment casting techniques, sacrificial polymeric objects are used to minimize costs and time to fabricate tooling used to make complex metal castings [17]. In a manner analogous to stereolithography or selective sintering, the LENS™ process builds metal parts line by line and layer by layer. This section will describe how LENS™ [10, 12, 18, 19] is utilized to fabricate metal components *directly* from CAD solid models and thus further reduce the lead times for metal part fabrication.

EXPERIMENTAL

As described in the previous section, a CAD solid model is sliced into a sequence of layers, and translated into a series of tool path patterns to build each layer. Each layer is fabricated by first generating an outline of the key component features and then filling the cross section using a rastering technique. This file is used to drive the laser system to produce the desired component one layer at a time, starting from the bottom of the part. A schematical representation of the LENS™ fabrication process is shown in Figure 1. A solid substrate is used as a base for building the LENS™ object. The laser beam is focused onto the substrate to create a weld pool in which powder particles are simultaneously injected to build up each layer. The substrate is moved beneath the laser beam to deposit a thin cross section, thereby creating the desired geometry for each layer. After deposition of each layer, the powder delivery nozzle and focusing lens assembly is incremented in the positive Z-direction, building a three dimensional component layer additively. To ensure that a uniform deposition was achieved for each layer independent of direction, a specialized powder delivery nozzle and powder feeder have been developed.

COMPONENT FABRICATION

After determining the basic LENS™ parameters for a material, a hollow geometry is typically fabricated. Figure 5 is a picture of an H13 tool steel part. The tallest geometry we can build in the LENS™ platform is 12 inches. For this geometry and material, the dimensional variance along Z is only 0.002 inches for the wingspan section of the thunderbird. The surface finish on extruded shapes is typically 250 μinch.

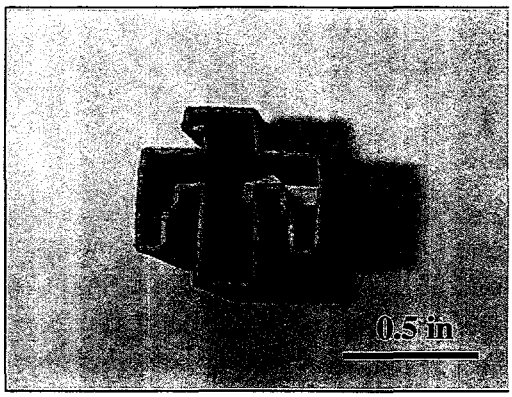

Figure 5. Thin-walled geometry fabricated from H13 tool steel.

From our understanding of the LENS™ parameters, solid geometries are fabricated. With a solid geometry, understanding the hatch spacing (line-by-line spacing) is critical for building 100% dense components. Figure 6 shows a housing (diameter = 1.5") built out of 316 stainless steel (SS316). This part is very accurate in X and Y dimensions, but the build height needs better control. The error in X and Y is less than ±0.005". However, Z can vary by as much as ±0.015" where the substrate extracts the thermal energy from the first few layers. By understanding the thermal behavior along with the LENS™ parameters, we should be able to control the Z height.

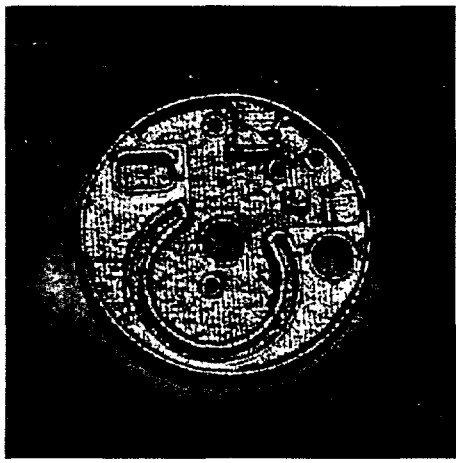

Figure 6. Solid geometry fabricated from 316 stainless steel.

Currently this process is being developed as a free-form fabrication process in which no support structures are needed. For a three-axis system, angle build studies suggest that the maximum angle, which can be achieved in a single-width deposition, is approximately 30° and about 15° for solid parts. A horizontal rotation axis has been added to the LENS™ system, and test geometries have been fabricated to show that a 90° bent pipe can be fabricated.

Although visual analysis of sample cross sections exhibited no obvious signs of porosity, helium pycnometry, Archimedes' method, and ultrasonic imaging were used to quantify the density for LENS™ processed materials. Both the pycnometry and Archimedes method showed the LENS™ processed materials to be fully dense. Ultrasonic imaging showed that the SS316 processed material had a few microvoids on the order of 1-5 μm in the interior of the solid. Electron microprobe analysis indicated that there was no apparent difference in composition between the deposited material and the original substrate (which is same material).

ACCURACY

Photographs of tolerance test parts used to measure the dimensional accuracy of the LENS™ process are shown in Figures 7 and 8. In building these components, it was determined that the dimensions in the X-Y plane could be maintained to less than ±0.002 inches (0.05 mm). The dimension in the Z or growth direction could only be maintained within ±0.015 inches (0.4 mm). The angle in the pyramid of Figure 6 is maintained within ±0.015 inches (0.4 mm). These results are extremely promising and further work will allow improvements in the dimensional accuracy to be achieved. The surface finish appears to be a strong function of the powder particle size with the smaller powder particles giving a better surface finish. Although the surface finish of the "as-built" component is somewhat rough, a small amount of finishing produces an accurate, high-polished surface.

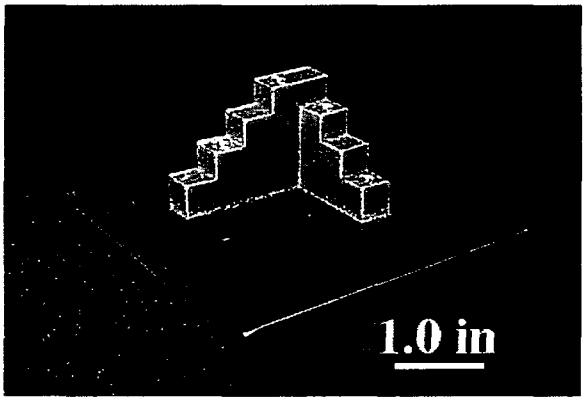

Figure 7. Accuracy test part with step geometry and cylindrical holes.

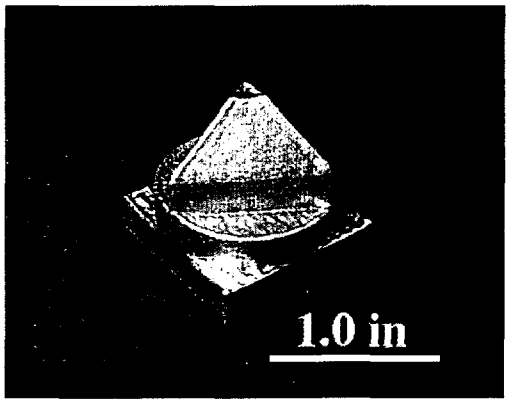

Figure 8. Square-circle-pyramid accuracy test part.

MECHANICAL TESTING

Results from tensile testing of the deposited 316 stainless steel are given in Table 2. Eight bars were tested, six with the layers perpendicular to the tensile pull direction, and two samples with the layers parallel to the tensile pull direction. A third set of data is given for conventionally processed, annealed 316 stainless steel. In all cases, the strength properties of the fabricated 316 stainless steel bars significantly exceed that for the reported value of the annealed material. The elongation for the LENS™ fabricated have

similar ductility where an elongation of 50% (in 1 inch) is achieved. Particle size did not affect the strength properties.

Table 2. Mechanical tensile test results for LENS™ fabricated SS316 bars. Plane orientation represents the layer build style with respect to the tensile pull direction.

Plane Orientation (w.rt. tensile direction)	Yield Strength (ksi)	Ultimate Tensile Strength (ksi)	Elongation% (in 2.54 cm)
perpendicular (-325 mesh)	65	115	66
perpendicular (+100/-325 mesh)	65	115	51
parallel (-325 mesh)	86	117	33
annealed bar	35	85	50

Metallographic cross sections of volumetric LENS™ fabricated parts exhibit no textured grain growth across the deposition layers. Moreover, Poisson's ratio is isotropic, and the tensile results do not show any preferred properties for specimens made with the layers perpendicular or parallel to the pull direction.

Similar results are seen for the Inconel 625 mechanical test results (Table 3), where high strength is achieved through grain-size refinement, but the ductility is not sacrificed.

Table 3. Mechanical tensile test results for LENS™ fabricated Inconel 625 bars.

Processing Style	Yield Strength (ksi)	Ultimate Tensile Strength (ksi)	Elongation% (in 2.54 cm)
LENS™	92	135	38
wrought	58	121	37

CONCLUSIONS FOR PART FABRICATION AND PROPERTIES

The feasibility of fabricating fully dense, solid metallic components directly from a CAD solid model has been demonstrated. The material properties obtained using alloys such as the Inconel 625 and 316 stainless steel are comparable to a conventionally processed wrought material. In some cases the material properties obtained in the LENS™ fabricated structure far exceed those for annealed materials. Dimensional studies have shown that very precise tolerances can be achieved in the horizontal build plane and the data generated from these studies has suggested ways to control and improve dimensional accuracy in the vertical fabrication direction. Further work is under way to continue to improve the material surface finish, and modified fabrication techniques are being explored to overcome angular limitations imposed by the current fabrication approach.

MULTIMATERIAL PROCESSING BY LENS™

INTRODUCTION

To advance direct fabrication capabilities, a process must be able to accommodate a wide range of materials, including alloys and composites. This is important for tailoring certain physical properties critical to component performance. Examples include graded deposition for matching coefficient of thermal expansion between dissimilar materials, layered fabrication for novel mechanical properties, and new alloy design where elemental constituents and/or alloys are blended to create new materials. In this section, we will discuss the development of precise powder-feeding capabilities for the LENS™ process to fabricate graded or layered material parts. We also present preliminary results from chemical and microstructural analysis.

MULTIMATERIAL POWDER FEED

Development of accurate powder-feeding capabilities is required for precise control of material placement. Previously, the LENS™ process fed powder into the molten pool for accurate control of line height over a narrow range of flow conditions. The powder feeder was redesigned for accurate flow conditions over a large range of flow rates. Moreover, computer control was integrated into the powder feed system for unattended operation during fabrication of parts. Diagnostic testing was used to test powder-feeder designs and to study line heights to determine flow over a variety of feed conditions. Figure 9 shows a comparison between two powder feeders versus flow rates for a chosen laser power and traverse speed. The powder feeders correspond reasonably well, where both feeders show a linear change in line height for increasing powder flow rate. This linear change is beneficial for controlling powder blending or grading in multimaterial fabrication.

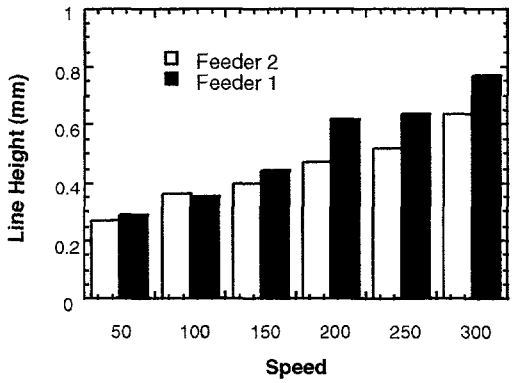

Figure 9. Line build height versus powder flow rate for redesigned powder feeders 1 & 2.

Graded samples consisted of precise deposition where material A was homogeneously deposited, then material B was slowly blended into A from 0 to 100 volume percent (v/o), and lastly material B was fabricated on top. For this study material A is stainless steel 316 (SS316), and material B is Inconel 690 (In690). Further work into graded, and layered fabrication can be found in more detail elsewhere [20].

Samples were cross sectioned, polished, and etched. Optical microscopy and scanning electron microscopy (SEM) were used to evaluate microstructure and porosity. Quantitative analysis of elemental constituents was determined with electron microprobe. Hardness was characterized by either Vickers or Rockwell techniques. Ferrite content in the microstructure was measured as Ferrite Number (FN) by a Magne gauge and ferrite scope.

RESULTS

Figure 10 shows the quantitative elemental constituent results for blending In690 into SS316. As expected, the iron (Fe) content decreases as In690 is added, resulting in increasing nickel (Ni) content. The elemental constituents match with values calculated using a simple rule of mixtures model. Processing conditions were not optimized, but the density of the sample was greater than 98%.

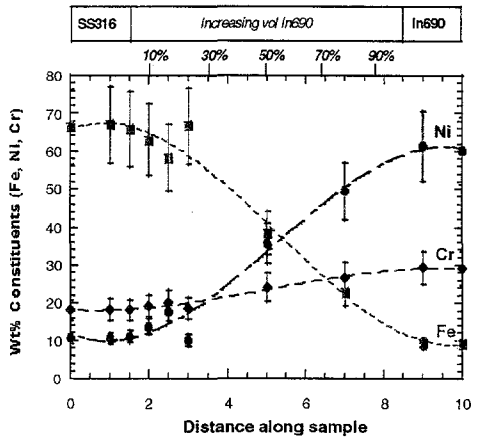

Figure 10. Alloyed constituent results for blending In690 into SS316 from 0 -100 volume percent.

Figure 11 shows the change in hardness over the graded sample. The hardness drops as small amounts of In690 are added to the SS316. At approximately 25 v/o In690, the hardness reaches a low value of 75 HRB. Beyond 25 v/o, the hardness increases until pure In690 is fabricated. This change in hardness at 25 v/o is due to a change in solidification mode. Pure SS316, as-processed by LENS™, begins solidifying as primary

ferrite. Upon cooling, the primary ferrite undergoes a phase change to austenite with a small amount (< 5%) retained skeletal ferrite, referred to as the "ferritic-austenitic solidification mode" [21]. In contrast, pure In690 solidifies by primary austenite solidification, with retained eutectic ferrite, otherwise known as the "austenitic-ferritic solidification mode" [21].

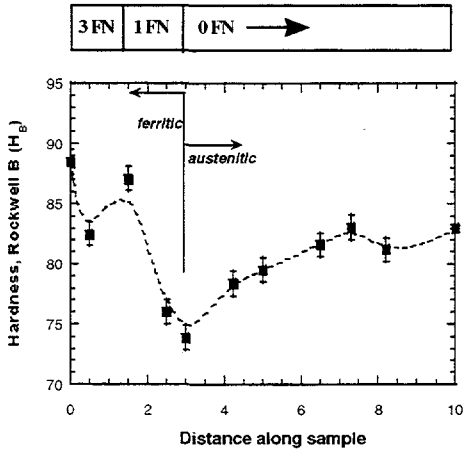

Figure 11. Hardness values for graded structure from Figure 10.

Figure 11 shows the change in the skeletal ferrite as measured by ferrite number (FN). In the pure SS316, the ferrite content is approximately 3 FN. This decreases as In690 is graded into the mixture. In the range of 20-30 v/o In690, the skeletal ferrite disappears because of the changing solidification mode (ferritic-> austenitic) and FN = 0. Moreover, the decreasing iron content along with changes in the Cr/Ni equivalency ratio convert the solidification mode from the primary ferritic to the primary austenitic solidification mode. Beyond 25 v/o In690, the hardness increases linearly through solid solution of Ni and Cr additions.

CONCLUSIONS FOR MULTIMATERIAL DEVELOPMENT

In summary, a new powder-feeder design allows for controlled flow, where dense parts were fabricated in graded structures. Microstructure and hardness could be tailored when blending In690 into stainless steel 316. With this initial work complete, studies of phase formation, microstructural development, and property tailoring have the potential for unique fabrication of components by LENS™ processing. Future work will require further software development to control material placement during part fabrication.

SOFTWARE DEVELOPMENT

INTRODUCTION

For any layered manufacturing technology, the overall goal of the control software is to take a CAD representation of the part, slice the model into appropriate thickness layers, and create path instructions for the manufacturing equipment. For LENS™, the path planning process begins with an object defined using the stereolithography (STL) format. This triangulated mesh is intersected with appropriately defined planes in order to create two-dimensional contour information for each layer to be formed. These contours are then refined to remove any vertex redundancies and to improve part quality. After cleanup, if creating a solid part, the contours are used as a basis for creating the necessary fill pattern. The final result of the path planning process is a tool path program (G-code) that is used to drive the three axes of the LENS™ machine.

Recent research into LENS™ has highlighted the sensitivity of the processes to multiple software controllable parameters such as substrate travel velocity, border representation, and fill patterns. Software development is aimed at determining optimal border outlines and fill patterns for LENS™ and at developing the associated software necessary for automating the creation of the desired motion control.

FILE FORMAT USED BY LENS™

As previously stated, the LENS™ process starts with an object defined through the rapid prototyping industry standard STL format. While the deficiencies of this format are well understood, the use of STL meshes for object definition does allow a large variety of CAD packages to be used to develop parts for use with LENS™. Furthermore, the simple triangular format used by STL allows for relatively easy manipulation of the part files. While the STL format is typically not a precise representation of the original CAD model (curved surfaces are faceted), meshes can be readily cut. The meshes are well within the tolerances of the LENS™ process. The only true difficulty posed by the use of the STL format is that the triangular representation, when sliced, often results in vertex redundancies (straight edges defined by more than two vertices, arcs being "over defined," etc.). As will be discussed, these redundancies will often have adverse affects on the build process. To minimize these affects, the contours require significant refinement.

CONTOUR REFINEMENT

Because of the nature of triangular meshes, when intersecting a mesh with a plane to create a two-dimensional contour, the vertices formed from the intersection process will inevitably contain numerous "redundant" vertices—vertices that do not add information about the contour's geometry or topology. Even for a simple cube, as shown

in Figure 12, a straightforward intersection of any plane with the triangular mesh will create line segments that contain more than the minimum two vertices. While these redundancies may not pose problems for other layered manufacturing processes, they may significantly affect the quality of parts produced through the LENS™ process. Primarily, each line segment start/stop reduces the physical machine speed as the stages are forced to decelerate and accelerate through each vertex. Since the LENS™ build rate is related to laser energy per unit time, decreasing the stages' velocities results in a significant alteration of the metal deposition.

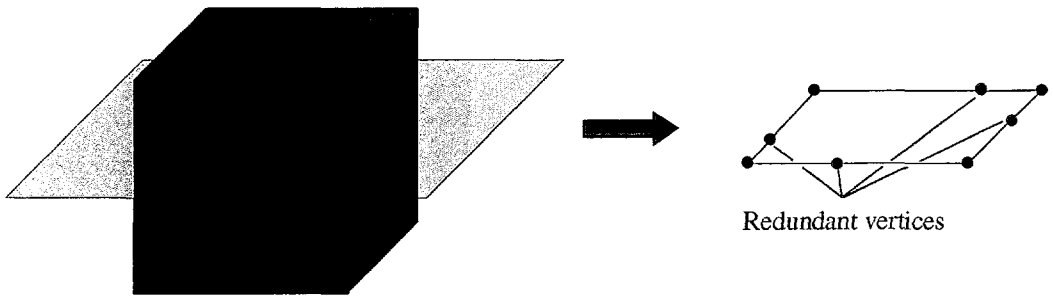

Figure 12. Intersection of a triangular mesh with a plane typically results in a 2D contour with redundant vertices.

Another obstacle, resulting from the use of a triangulated mesh to define the object, is a possible "over refinement" of arcs and circles. As with over-defined straight segments, the accelerations and decelerations through each vertex of an over-defined arc results in a decrease in the travel speed and a corresponding increase in the metal deposition rate (Figure 13(a)).

The contour-refinement process is relatively straightforward. First, any duplicate vertices are removed from the contour. (Duplicate vertices are considered as those that are coincident to each other within some epsilon.) Second, any redundant vertices are located and removed from line segments. To locate the redundant vertices, the included angle of the two-line segments that share each vertex is computed. Any vertex whose included angle is greater than a user-defined value (typically around 179°) is removed. It should be noted that this process also eliminates excessive vertices in arcs or other curve segments. It is also possible at this stage to locate any arcs or circles in the contour representation and replace the segmented representation with appropriate second order formulations. As shown in Figure 13(b), dramatic improvements in part quality are obtained through proper contour refinement.

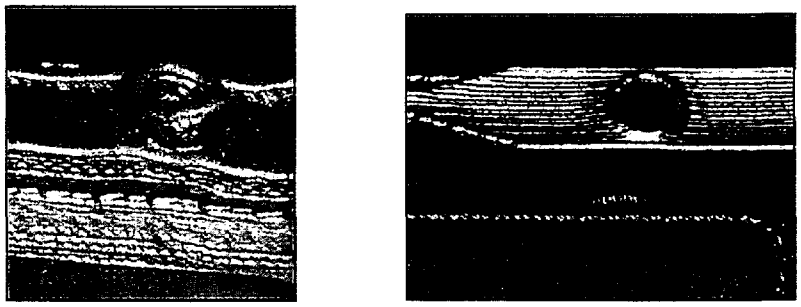

(a) (b)

Figure 13. Contour refinement examples: (a) using too many edges to define contours results in excessive buildup. (b) reducing the number of edges used to define the contour produces a more desirable part.

FILL PATTERN

For solid parts, an appropriate technique must be used to create the necessary fill pattern. The choices for this fill technique may be broken down into one of two primary methods: rasters and "conformal" contours. Regardless of method, the fill technique must meet one primary requirement. Since the metal for material buildup is injected into the LENS™ part as a powder stream, effects of the localized geometry on the powder stream must be controlled. Furthermore, it must be recognized that the weld beads have finite width; widths that may not always "fit" evenly into a layer's border geometry, causing both regions of excessive overlap and possible voids (Figure 14). For even basic geometry, many problems may be encountered during a fill pass. Since the width of the weld pool will not always produce weld bead edges aligned with the border geometry, regions of large overlap, and regions with voids may be formed. Further, gas currents blowing back from the part may affect the powder stream, especially in tight areas. If the same fill pattern is repeated, the small disturbances produced by these flaws will build upon themselves, resulting in a poor final product. While neither overlaps nor voids are in and of themselves detrimental to the build process (overlaps will produce a slight increase in thickness, while voids will result in a slight decrease), the errors caused by these localized flaws can, if compounded across enough layers, will result in a poor part. Attacking the geometry from different directions during the fill process can alleviate the localized effects. To accomplish the different angles of attack, the fill pattern must be designed such that a "randomness" is introduced into the build process.

Conformal contours, which follow the outline of the part in decreasing size, were studied as one possible fill technique. However, basic experiments with conformal contours revealed that even for simple cylindrical parts, the required randomness is not introduced, resulting in extremely poor builds (Figure 15a).

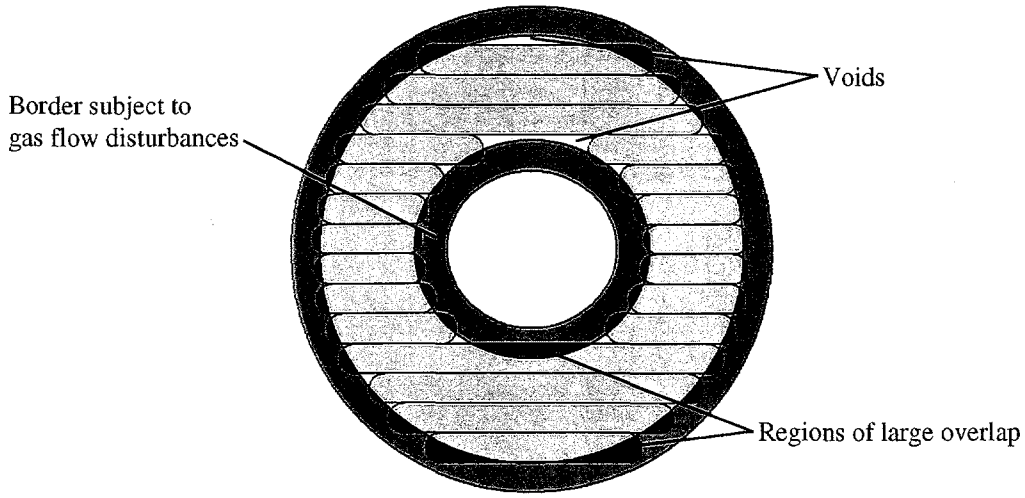

Figure 14. Fill pattern issues: weld beads have finite width; widths may not always "fit" evenly into a layer's border geometry causing regions of excessive overlap and possible voids.

The use of raster fills has proven an effective method of introducing the necessary variations between the fill vectors on each layer. However, even here, care must be exercised when determining the raster angles on a per layer basis. Early work on LENS™ utilized rasters that were always oriented at either 0° or 90°. While a vast improvement over the use of conformal contours, these static angles were still the source of localized build errors, because of the repetition of the fill angles. As a result, regions aligned with the *x* and *y*-axes would often experience unevenness in the build (Figure 15b).

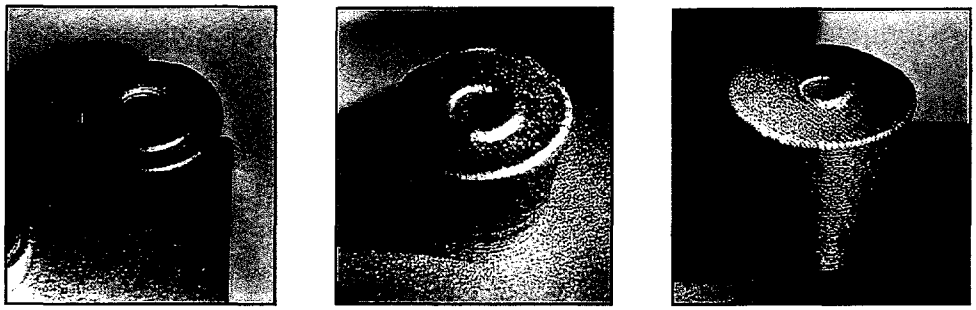

Figure 15. Fill pattern styles: (a) created using conformal contours. (b) created using a 0°, 90° raster hatch pattern. (c) created using a 0°, 105°, 220°, ... hatch pattern.

The first attempt at introducing more variation into the hatch angles was to use randomly generated values for the hatch orientations. However, this allowed for angles that are just a few degrees off of the "standard" angles of 0°, 30°, 45°, 60°, and 90°.

When filling near these standard angles with a shallow angle of attack (e.g., filling along a 30° border with a 31° hatch angle), the width of the weld bead repeatedly overlaps the border, producing a significant buildup, again resulting in an uneven build, as demonstrated in Figure 16. Furthermore, retracting the hatch to prevent the overlap was undesirable due to the likelihood of forming voids in the part.

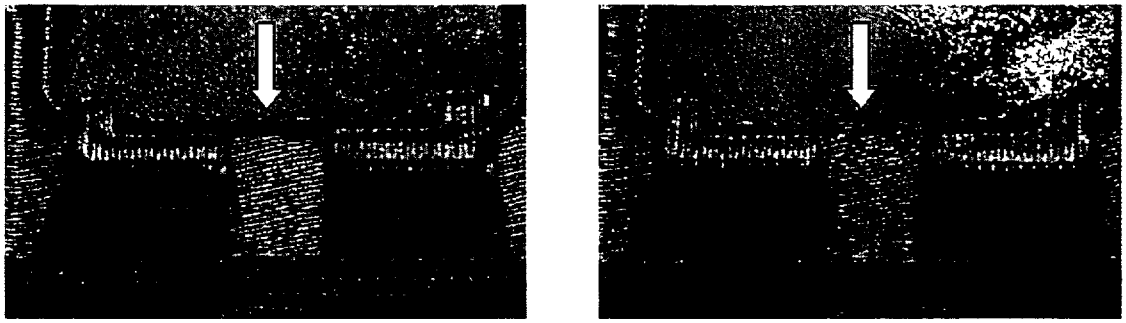

(a) (b)

Figure 16. (a) Shallow angles of attack between border vectors and the fill rasters produce buildup along borders. (b) Eliminating these shallow attack angles produces improved characteristics.

After several iterations, the angle pattern converged on using a value of 105° between successive layers. This value provided several key benefits:

1. The fill angles across two layers are nearly orthogonal, allowing for a large differentiation of attack angle to minimize the localized geometry effects.

2. Also, at 105°, it takes 12 layers before any raster angle is repeated in a part, which further introduces pseudo-randomness into the process.

3. Finally, 105° causes the standard angles to be either hit exactly, or at an angle greater than or equal to 15°, preventing the shallow angle of attack problems previously discussed.

As shown in Figure 15(c) and Figure 16, the results obtained through the 105° hatch algorithm are significantly improved over both 0°, 90° hatching and conformal contours. Details about this work can be found elsewhere [22].

CONCLUSIONS FOR SOFTWARE DEVELOPMENT

Recent experience in LENS™ has demonstrated the strong reliance that the metal deposition process has two parameters such as border representations and fill patterns. This research was aimed at understanding and developing optimized software solutions for the generation of LENS™ parts. Specifically, this work studied the effects of the border representation schemes, identified difficulties associated with over-defined representations, and developed methods of refining the contour data to improve the build process. Furthermore, this research was directed at identifying an "ideal" fill pattern for creating solid parts. The final result of the fill pattern studies produced pseudo-random raster fill technique that introduces the necessary randomness into the build process to minimize localized geometry effects, while preventing problems with shallow angles of attack along standard design surfaces.

SUMMARY

Through this LDRD project, we have achieved a fundamental understanding of the LENS™ process. We understand the relationship between the processing variables (power, speed, powder feed rate) and the resulting properties (density, accuracy, strength, ductility). With this understanding, we have been able to fabricate various components, from extrusion shapes to prototype solids. We have complete feasibility studies for Defense Programs' applications including discriminator housing, crystal housing, and tooling.

Further development of this technology will provide component groups with a new technology to use in development of improved materials and hardware functionality for stockpile support. In addition to rapid manufacturing operations, this technology provides a unique process that can be used for direct metal deposition with a minimum dilution of the existing substrate material. This has a direct benefit in joining or repair operations.

A final derivative of this process will be the capability to produce new classes of materials. Initial experiments have concluded that LENS™ can produce graded as well as composite structures. Development of this process has the potential to open up an exciting new area for advanced materials development and provide unique materials for weapons applications.

References

1. A. Frenk and J. D. Wagniere, "Laser Cladding with Cobalt-Based Hardfacing Alloys," J. Phys. IV, **1** (1991) p c7-65.

2. R. Subramanian, S. Sircar and J. Mazumder, "Laser Cladding of Zirconium on Magnesium for Improved Corrosion Properties," J. Mater. Sci. **26** (1991) p 951.

3. K. M. Jasim, R. D. Rawlings and D. R. F. West, "Thermal Barrier Coatings Produced by Laser Cladding," J. Mater. Sci. **25** (1990) p 4943.

4. J. De Damborenea and A. J. Vazquez, "Laser Cladding of High-Temperature Coatings," J. Mater. Sci. **28** (1993 p 4775.

5. S. Sircar, K. Chattopadhyay and J. Mazumder, "Nonequalibrium Synthesis of $NbAl_3$ and Nb-Al-V Alloys by Laser Cladding: Part I. Microstructure Evolution," Metall. Trans. A **23A** (1992) p 2419.

6. J. Mazumder and A. Kar, "Solid Solubility in Laser Cladding," J. Met. (Feb. 1987) p 18.

7. Y. Kizaki, H. Azuma, S. Yamazaki, H. Sugimoto and S. Takagi, "Phenomenological Studies in Laser Cladding. Part I. Time-Resolved Measurements of the Absorptivity of Metal Powder," Jpn. J. Appl. Phys. **32** (1993) p 205.

8. Y. Kizaki, H. Azuma, S. Yamazaki, H. Sugimoto and S. Takagi, "Phenomenological Studies in Laser Cladding. Part II. Thermometrical Experiments on the Melt Pool," Jpn. J. Appl. Phys. **32** (1993) p 213.

9. J. L. Koch and J. Mazumder, "Rapid Prototyping by Laser Cladding," ICALEO '93 Proc. **77** (1993) p 213.

10. D. M. Keicher, J. A. Romero, C. L. Atwood, J. G. Smugeresky, M. L. Griffith, F. P. Jeantette L. Harwell and D. Greene, "Laser Engineered Net Shaping (LENS™) for Additive Component Processing," Rapid Prototyping and Manufacturing '96 Proc., April 1996.

11. U.S. Patent #4,323,756, "Method for Fabricating Articles by Sequential Layer Deposition," (To Pratt and Whitney).

12. D. M. Keicher, J. L. Jellison, L. P. Schanwald, J. A. Romero and D. H. Abbott, "Towards a Reliable Laser Powder Deposition System Through Process Characterization," SAMPE '95 Proc. p1029.

13. M. Burns, Automated Fabrication: Improving Productivity in Manufacturing, Prentice Hall, Englewood, NJ, (1993).

14. T. Wohlers, "State of the Industry," Proceedings of the Rapid Prototyping & Manufacturing '96 Conference, published by the Society of Manufacturing Engineers, Dearborn, MI, (1996).

15. P. Jacobs, Rapid Prototyping and Manufacturing: Fundamentals of Stereolithography, published by the Society of Manufacturing Engineers, Dearborn, MI, (1992).

16. K. McAlea, R. Booth, P. Forderhause, U. Lakshminarayan, "Materials for Selective Laser Sintering Processing," 27th International SAMPE Technical conference, Vol. 27, Diversity into the Next Century, proceedings of SAMPE '95, Albuquerque, NM, October 12-14, 1995, p. 949.

17. M. D. Baldwin, C. L. Atwood, and M. C. Maguire, "Integration of Rapid Prototyping into Investment Casting," Proceedings of the Rapid Prototyping & Manufacturing '95 Conference, published by the Society of Manufacturing Engineers, Dearborn, MI, (1995).

18. D. M. Keicher, J. A. Romero, C. L. Atwood, J. E. Smugeresky, M. L. Griffith, F. P. Jeantette, L. D. Harwell and D. L. Greene, "Free Form Fabrication using the Laser Engineered Net Shaping (LENS™) Process," Proceedings of the 1996 World Congress on Powder Metallurgy and Particulate Materials, Advances in Powder Metallurgy, published by the Metal Powder Industries Foundation, Princeton, NJ.

19. M. L. Griffith, D. M. Keicher, C. L. Atwood, J. A. Romero, J. E. Smugeresky, L. D. Harwell, D. L. Greene, *Free Form Fabrication of Metallic Components using Laser Engineered Net Shaping (LENS™)*, Proceedings of the Solid Freeform Fabrication Symposium, August 12-14, 1996, Austin, TX, p.125.

20. M. L. Griffith, L. D. Harwell, J. A. Romero, M. E. Schlienger, C. L. Atwood, J. E. Smugeresky, *Multi-Material Processing by LENS™*, Proceedings of the Solid Freeform Fabrication Symposium, August 1997, Austin, TX.

21. J. A. Brooks, J. C. Lippold, *Selection of Wrought Austenitic Stainless Steels*, ASM Handbook Volume 6: Welding, Brazing, and Soldering, published by the American Society of Metals, 1993, p. 456.

22. M. T. Ensz, M. L. Griffith, *Software Development for Laser Engineered Net Shaping*, proceedings of the Solid Freeform Fabrication Symposium, August 1998, Austin, TX.

Distribution:

1	MS0149	Chuck Meyers, 4000
1	MS0188	Donna Chavez, 4001
1	MS0340	Tony Romero, 1831
5	MS0958	Clint Atwood, 1484
1	MS0958	Mark Ensz, 1484
5	MS0958	Michelle Griffith, 1484
1	MS0958	Lane Harwell, 1484
1	MS0958	Donald Greene, 1484
1	MS0958	Daryl Reckaway, 1484
1	MS0958	Bruce Swanson, 1484
1	MS0959	Jon Munford, 1492
1	MS0960	Jimmie Searcy, 1400
5	MS9403	John Smugeresky, 8712
1	MS1411	Mike Oliver, 1831
5	MS1411	Duane Dimos, 1831
1	MS1434	Jim Jellison, 1803
1	MS1452	Francisco Jeantette, 4423
1	MS9018	Central Technical Files, 8940-2
2	MS0899	Technical Library, 4916
1	MS0619	Review & Approval Desk, 15102 For DOE/OSTI